Computational Materials Science 85 (2014) 8–15

Contents lists available at ScienceDirect

Computational Materials Science

journal homepage: www.elsevier.com/locate/commatsci

Hydrostatic pressure effects on deformation mechanisms of nanocrystalline fcc metals

Fuping Yuan *, Xiaolei Wu

State Key Laboratory of Nonlinear Mechanics, Institute of Mechanics, Chinese Academy of Science, Beijing 100190, People's Republic of China

ARTICLE INFO

Article history:
Received 23 October 2013
Received in revised form 10 December 2013
Accepted 20 December 2013
Available online 11 January 2014

Keywords:
Molecular dynamics
Nanocrystalline metals
Hydrostatic pressure

ABSTRACT

A series of large-scale molecular dynamics (MD) simulations have been performed to investigate hydrostatic pressure effects, and the interplay between pressure and grain size, on the flow stress and the related atomic-level deformation mechanisms in nanocrystalline (NC) Cu. The strength of NC Cu increases with increasing hydrostatic pressures for all grain sizes studies in the present paper (3–15 nm). The critical grain size for maximum strength first shifts towards lower values with increasing hydrostatic pressure (0–5 GPa), and then shifts towards higher values as the hydrostatic pressure becomes even higher (5–80 GPa). Below the critical hydrostatic pressure, the dislocation behaviors increase with increasing hydrostatic pressure for all grain sizes and the dependency of effective modulus as a function of hydrostatic pressure is almost the same for all grain sizes, which should lead to the position shifting of maximum strength towards lower grain sizes. Above the critical hydrostatic pressure, the dislocation behaviors start to decrease with increasing hydrostatic pressure for small grain sizes, and continue to increase with increasing hydrostatic pressure for large grain sizes. The slopes of effective modulus as a function of hydrostatic pressure increase slightly with increasing grain size above the critical hydrostatic pressure. The position shifting of maximum strength towards larger grain sizes at large hydrostatic pressure should be attributed to these two observations. Moreover, GB thickening is observed to increase monotonically with increasing pressure for all grain sizes, and the NC Cu with 3 nm grain size has the trend to become amorphous state under hydrostatic pressure of 80 GPa, which gives a new way to produce crystalline-to-amorphous transition. The findings in the present study should provide insights to the potential applications of NC metals under extreme environments.

© 2013 Elsevier B.V. All rights reserved.

1. Introduction

Nanocrystalline (NC) metals (grain size less than 100 nm) have attracted considerable interests due to many unique mechanical properties, such as increased strength/hardness, improved toughness and enhanced diffusivity compared to coarse grained counterparts [1,2]. The strength/hardness has been found to increase with decreasing grain size down to a critical value (10–20 nm), following the well known Hall–Petch (H–P) relation. The increased strength/hardness has been attributed to the increased area fraction of grain boundaries (GBs), which act as strong barriers to dislocation gliding. However, both experiments and simulations [3–14] have also shown that the strength/hardness decreases with further grain refinement below the critical value (10–20 nm), suggesting that dislocation activities give way to GB-associated plasticity such as GB sliding, GB diffusion and grain rotation. Moreover, twin boundary spacing (TBS) has been found to affect the strength of nanotwinned (NT) Cu in a similar way [15–22]. The strength of NT Cu has been found to first increase with decreasing TBS, reaching a maximal strength at a critical TBS, then decrease with further reduced TBS. However, the softening trend below the critical TBS for NT Cu has been attributed to a dislocation-nucleation-controlled softening mechanism with twin-boundary migration [18], not necessarily related to GB-mediated process.

It is now commonly accepted that interplay between dislocation activities and GB process controls the intrinsic deformation behavior and strength of NC metals. Harder materials could be created if softening effects, such as GB process, could be suppressed under extreme environment. However, the precise trade-offs between these two deformation mechanisms are still unclear, especially the effects of pressure on these two mechanisms are still vague [21,23–27]. Bringa et al. [23] have studied pressure effect on the shock compression of NC Cu. An ultra-high strength behind the shock front was observed due to the high pressure and the suppression of GB sliding under shock loading. As pressure increased, a shift in the maximum strength to lower grain sizes was observed due to the suppression of GB associated plasticity. However, beyond a critical pressure, higher temperatures due to adiabatic heating resulted in a drop in strength. In our previous study [21],

* Corresponding author. Tel.: +86 10 82544409; fax: +86 10 82543977.
E-mail address: fpyuan@lnm.imech.ac.cn (F. Yuan).

0927-0256/$ - see front matter © 2013 Elsevier B.V. All rights reserved.
http://dx.doi.org/10.1016/j.commatsci.2013.12.047

an ultra-high strength behind the shock front has also been found in NT Cu due to increased dislocation behaviors. Under shock loading conditions, the uniaxial loading is carried by a shock wave traveling faster than the sound velocity, pressure builds up along with inhomogeneous deformation and temperature rise by adiabatic heating. In order to investigate the pressure effect solely, excluding the temperature and shock effects, uniaxial compression experiments under high hydrostatic pressure by the panoramic-type diamond anvil cell have been adopted [24,25,28]. Such deformation experiments at high pressure on polycrystalline nickel suggest that dislocation activity is still operative in 3 nm crystals [24]. The observations of pressure-promoted texturing indicate dislocation activity can be extended down to a few-nm-length scale under high external hydrostatic pressures [24]. In situ observation of plastic accommodation by dislocations and/or GB processes in NC metals is difficult due to technical limitations, and the extremely high hydrostatic pressures are also difficult to achieve by the set-up of diamond anvil cell. However, molecular dynamics (MD) simulations have proven to be particularly useful for investigating the plastic deformation mechanism of NC metals with carefully designed model system, in which the extremely high hydrostatic pressures can be easily build up by a Nose–Hoover barostat and the transient responses of the system can be examined [6,7,29,30]. The MD simulations should enable uncovering various deformation and microstructural processes in well-designed model systems, something that has proven difficult to achieve in experiments. In this regard, the focus of this paper is to understand the hydrostatic pressure effects and the interplay between pressure and grain size on determining the strength and the related atomic-level deformation mechanisms in NC Cu using MD simulations.

2. Simulation techniques

The MD simulations were carried out using the Large-scale Atomic/Molecular Massively Parallel Simulator (LAMMPS) code and a Cu EAM potential developed by Mishin et al. [31]. This potential has been extensively calibrated by calculating FCC lattice properties, point and extended defects, various structural energies, and transformation paths according to the corresponding experimental or ab *initio* values. These parameters for pure Cu metal are compared and shown in Table 1, where a_0 is lattice constant, B is bulk modulus, c_{11}, c_{12} and c_{44} are the corresponding elastic constants, γ_{SF} is intrinsic stacking fault (ISF) energy, γ_s is the surface energy for the corresponding planes, and γ_T is TB energy.

The initial three-dimensional polycrystalline Cu samples containing 27 grains with random orientations were created using the Voronoi polyhedral construction, in which most GBs are high-angle GBs. Seven grain sizes (d = 3.0, 5.0, 6.5, 8.0, 9.5, 11.0, 15.0 nm, determined from the mean length of the cube for the grain) were considered in order to investigate the grain size effect on the deformation behaviors of polycrystalline Cu. The sample with grain size of 15 nm has dimensions of $45 \times 45 \times 45$ nm^3, and contains approximately 7,800,000 atoms. The same Voronoi grain structure and the same crystallographic orientations of all grains were retained for all grain sizes. The typical relaxed NC Cu with grain size of 9.5 nm is shown in Fig. 1(a). Periodic boundary conditions were imposed along all three directions. Before loading, the as-created samples were first subjected to energy minimization by the conjugate gradient method, then gradually heated up to the desired temperature in a step-wise fashion, and finally relaxed in the Nose/Hoover isobaric–isothermal ensemble (NPT) under both the pressure 0 bar and the desired temperature (1 K) for 100 ps. The relaxed NC samples, initially at P = 0 GPa, were compressed up to the desired hydrostatic pressure P and relaxed at that pressure in the Nose/Hoover NPT ensemble until the volumes reached the equilibrium (Fig. 1(a)), and then were compressed to 15% at strain rate of 5×10^8/s along the x direction while keeping $\sigma_{yy} = \sigma_{zz} = P$ (Fig. 1(b)). Seven hydrostatic pressures (P = 0, 2, 5, 10, 20, 40, 80 GPa) were considered in order to investigate the pressure effect on the deformation behaviors of NC Cu.

Table 1
Comparison of parameters from experimental results and Mishin's potential for Cu.

	Exp.	EAM		Exp.	EAM
a_0 (Å)	3.615	3.615	γ_{SF} (mJ/m^2)	45	44.4
B (10^{11} Pa)	1.383	1.383	γ_s (111) (mJ/m^2)	1790	1239
c_{11} (10^{11} Pa)	1.700	1.699	γ_s (110) (mJ/m^2)	1790	1475
c_{12} (10^{11} Pa)	1.225	1.226	γ_s (100) (mJ/m^2)	1790	1345
c_{44} (10^{11} Pa)	0.758	0.762	γ_T (mJ/m^2)	24	22.2

The structural analysis was carried out at different times during the deformation. For this purpose, the pair correlation function and the common neighbor analysis (CNA) [32] were employed. The CNA is a tool used in atomistic simulations which allows us to determine the local ordering in a given structure. In CNA, nearest neighbors can be determined if the distance between them is less or equal to the cutoff distance, which is in general defined as the first minimum in the pair distribution function and is also lattice constant dependent (density dependent). The CNA not only considers the number of neighbors at a given distance but also their location with respect to other common neighboring atoms. With CNA one can distinguish atoms in FCC, HCP and BCC regions by calculating the statistics of diagrams formed from the nearest neighbors of each atom and comparing it with those previously known from standard crystals.

3. Results and discussions

As indicated earlier, the NC samples were first compressed at desired hydrostatic pressure P and relaxed at that pressure until the volumes reached the equilibrium. Under hydrostatic compression, the materials generally shrink in volume and the density of materials increases with increasing hydrostatic pressure. The relation between the hydrostatic pressure and the volume/density of a solid at a given temperature is generally called equation of state. Fig. 2(a) shows the relationship between the normalized density and the hydrostatic pressure at a given temperature of 1 K for NC Cu with various grain sizes. The densities for NC Cu at various hydrostatic pressures were normalized by the density of single crystal at 0 pressure and 1 K. It is interesting to note that the compressibility with increasing pressures is similar for all grain sizes. The fitting curve for the normalized density as a function of hydrostatic pressure can be obtained by least squares method and expressed as: $\rho_{norm} = 0.99477 + 0.00626P - 2.65361 \times 10^{-5}P^2$. Fig. 2(b) and (c) shows the simulated microstructural configurations for NC Cu with a grain size of 3 nm under zero hydrostatic compression and under hydrostatic compression at 80 GPa, respectively. Fig. 2(d) and (e) shows the simulated microstructural configurations for NC Cu with a grain size of 15 nm under zero hydrostatic compression and under hydrostatic compression at 80 GPa, respectively. GB thickening is observed for NC Cu with all grain sizes under hydrostatic compression and the thickness of GBs increase with increasing hydrostatic pressure. Moreover, no dislocation behaviors are observed under hydrostatic compression for NC Cu with all grain sizes, which is consistent with the classical plastic theory.

After hydrostatic compression, the NC samples were compressed to 15% at strain rate of 5×10^8/s along the x direction while keeping $\sigma_{yy} = \sigma_{zz} = P$. According to either Von Mises criteria or Tresca criteria, the equivalent stress under this stress state can be calculated by: $\sigma_{equivalent} = \sigma_{xx} - P$. The simulated stress–strain

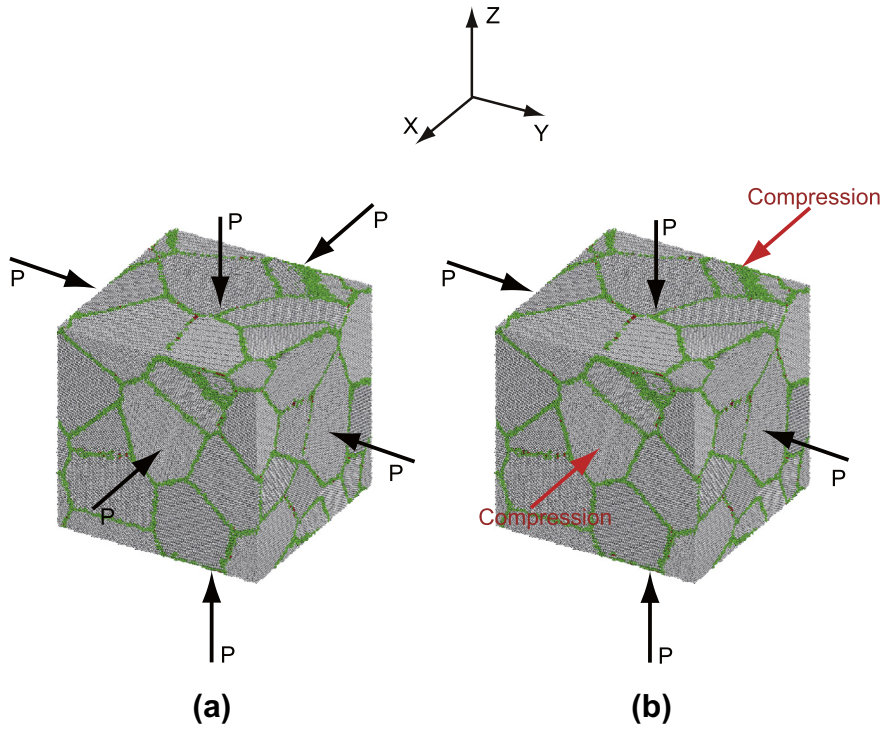

Fig. 1. The relaxed NC Cu with grain size of 9.5 nm: (a) was compressed up to the desired hydrostatic pressure P and relaxed at that pressure; (b) and then was compressed along the x direction while keeping $\sigma_{yy} = \sigma_{zz} = P$. Gray color stands for perfect FCC atoms, red color stands for HCP atoms and green color stands for grain boundaries (GBs), dislocation core, free surface and other atoms. The same CNA color coding is used in the all figures in the present study. (For interpretation of the references to color in this figure legend, the reader is referred to the web version of this article.)

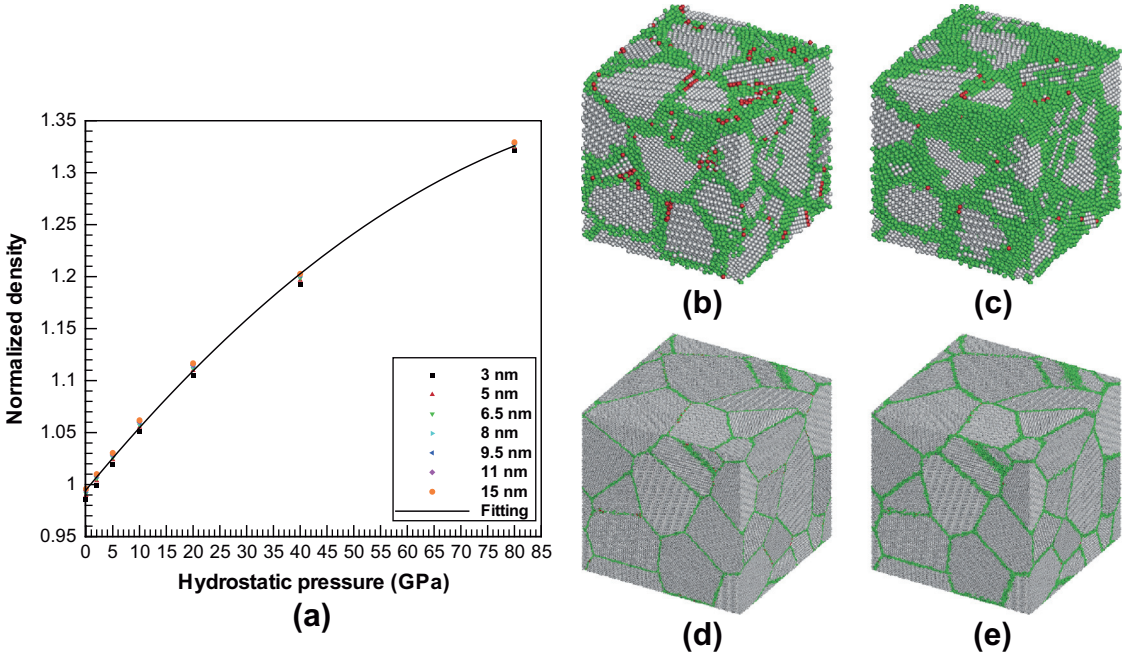

Fig. 2. (a) The normalized density vs. the hydrostatic pressure. The simulated microstructural configurations for: (b) NC Cu with a grain size of 3 nm without hydrostatic compression; (c) NC Cu with a grain size of 3 nm after hydrostatic compression at $P = 80$ GPa; (d) NC Cu with a grain size of 15 nm without hydrostatic compression; and (e) NC Cu with a grain size of 15 nm after hydrostatic compression at $P = 80$ GPa.

curves for NC Cu with various grain sizes under different hydrostatic pressures are shown in Fig. 3. In Fig. 3, The vertical ordinate represents the equivalent stress $\sigma_{equivalent}$, while the horizontal ordinate is the strain along the x direction. The equivalent stresses are observed to increase linearly first with strain at the elastic stage, and continue to increase nonlinearly to a certain peak stress at the initial plastic stage, and then gradually decrease to a steady-state value regardless of grain sizes and hydrostatic pressures.

In order to study the interplay between pressure and grain size on the flow stress, it is physically more meaningful to compare the average flow stress over a certain plastic strain interval due to the peak stress overshoot induced by the high strain rate employed in

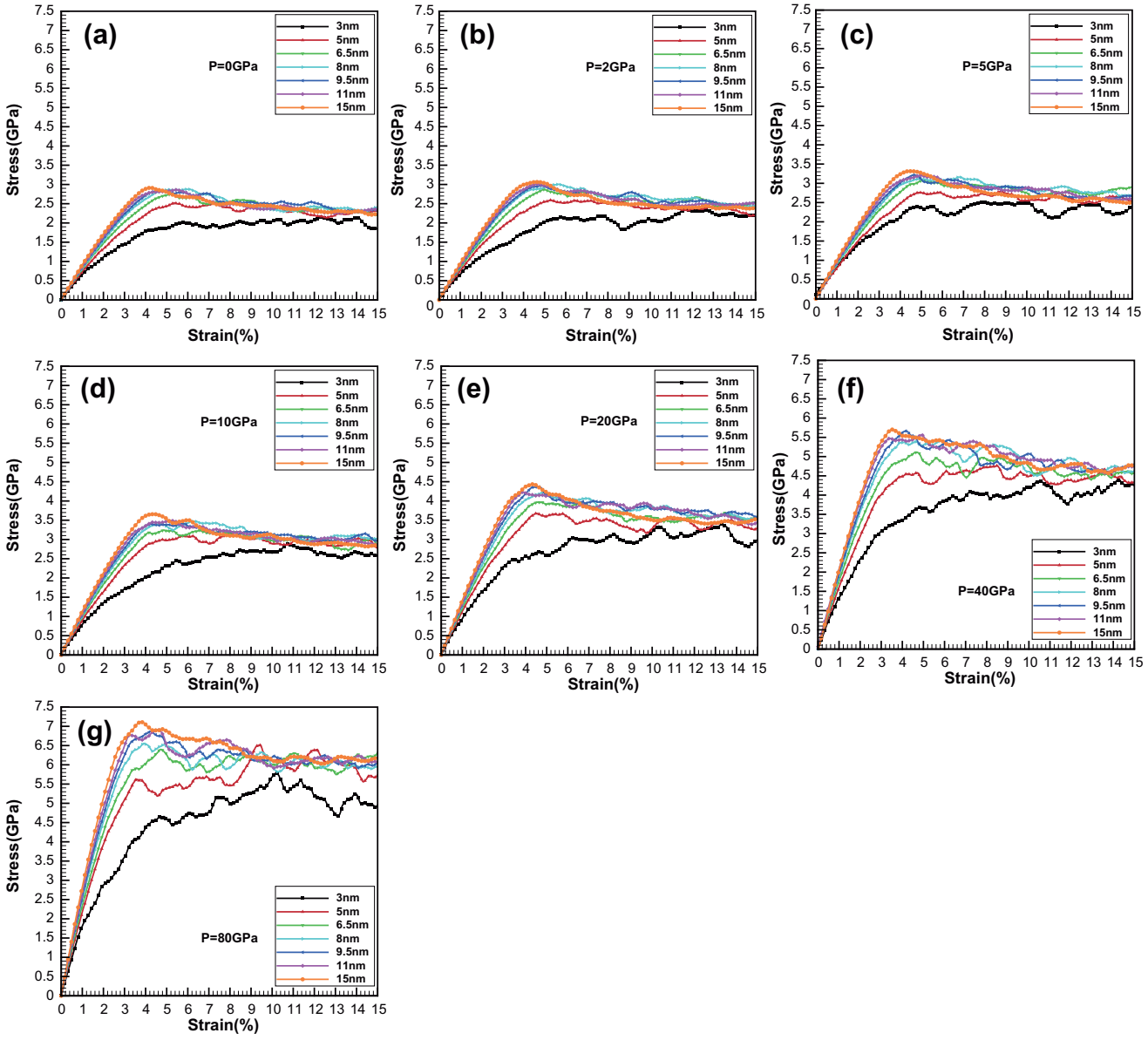

Fig. 3. The simulated stress–strain curves at 5×10^8/s under different hydrostatic pressures: (a) $P = 0$ GPa; (b) $P = 2$ GPa; (c) $P = 5$ GPa; (d) $P = 10$ GPa; (e) $P = 20$ GPa; (f) $P = 40$ GPa; and (g) $P = 80$ GPa.

MD simulations [6,14,18,33]. In view of this, the average flow stress from a strain of 10–15% is plotted against grain size for different hydrostatic pressures in Fig. 4(a). At zero hydrostatic pressure, it can be seen that the average flow stress first increases as grain size d decreases, reaching a maximum at a critical d, and then decreases as d becomes even smaller. This phenomenon can be explained by a shift in the dominated deformation mechanisms from dislocation-mediated plasticity to GB-associated plasticity such as GB sliding, GB diffusion and grain rotation when the grain size is refined to sub-10 nm regime. The critical grain size for maximum strength is at 9.5 nm under uniaxial compression loading, which is slightly smaller to the critical grain size under uniaxial tensile loading [6]. Moreover, the strengths of NC Cu increase with increasing hydrostatic pressure, and the critical grain size for maximum strength changes with increasing hydrostatic pressure, as shown in Fig. 4(b). It is observed that the critical grain size for maximum strength first shifts towards lower values with increasing pressure (0–5 GPa), and then shifts towards higher values as the hydrostatic pressure becomes even higher (5–80 GPa).

As mentioned earlier, the flow stress of NC metals is controlled by the interplay between dislocation activities and GB processes. Moreover, hydrostatic pressure has strong influence on both GB accommodation and dislocation activity. For pressure dependency, GB accommodation in NC metals has similarities to the plasticity of granular media [23,34,35], in which the onset of plasticity is generally predicted by the Mohr–Coulomb law of sliding friction. Associating the normal stress on the GB sliding with hydrostatic pressure, the flow stress for GB accommodation (GB sliding, etc.) can tentatively be written as: $\sigma_{GB} = (\sigma_0 + \alpha P)(1 + d/d_0)$, where σ_0, α and d_0 are material constants. Considering both hydrostatic pressure effects on effective modulus and the Hall–Petch relation, the flow stress for dislocation plasticity can be written as: $\sigma_{Disl} = C\overline{G}(d,P)(d/d_1)^{-0.5}$, where $\overline{G}(d,P)$ is the effective modulus for equivalent stress, C, d_1 are material constants [23]. The effective flow stress for a nanocrystal can be taken as $\sigma_{flow} = \min(\sigma_{Disl}, \sigma_{GB})$, however a more realistic model would include a mixture of both when $\sigma_{Disl} \sim \sigma_{GB}$ [23]. Both GB accommodation and dislocation plasticity mechanisms predict an increase in flow stress with

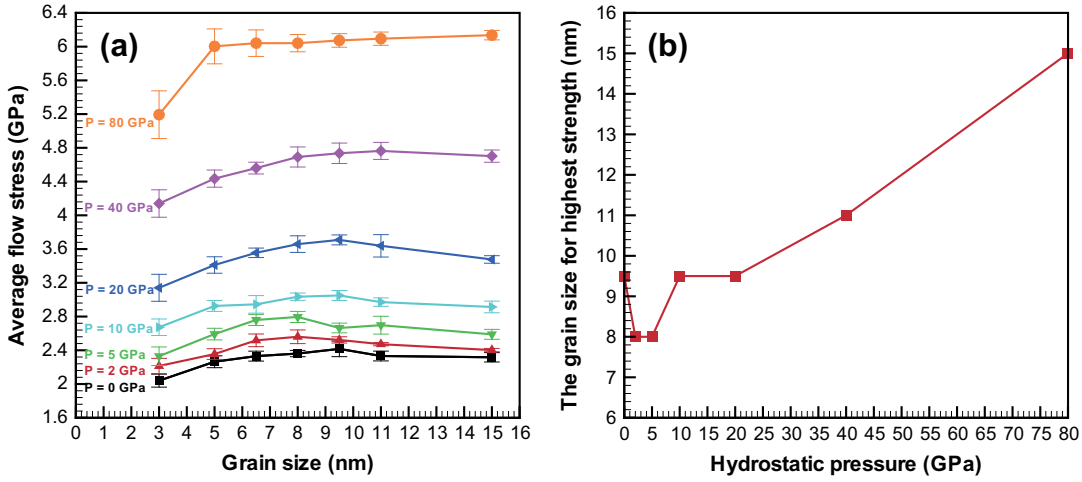

Fig. 4. (a) Average flow stress from a strain of 10–15% vs. grain size for different hydrostatic pressures; and (b) the critical grain size for maximum strength vs. hydrostatic pressure.

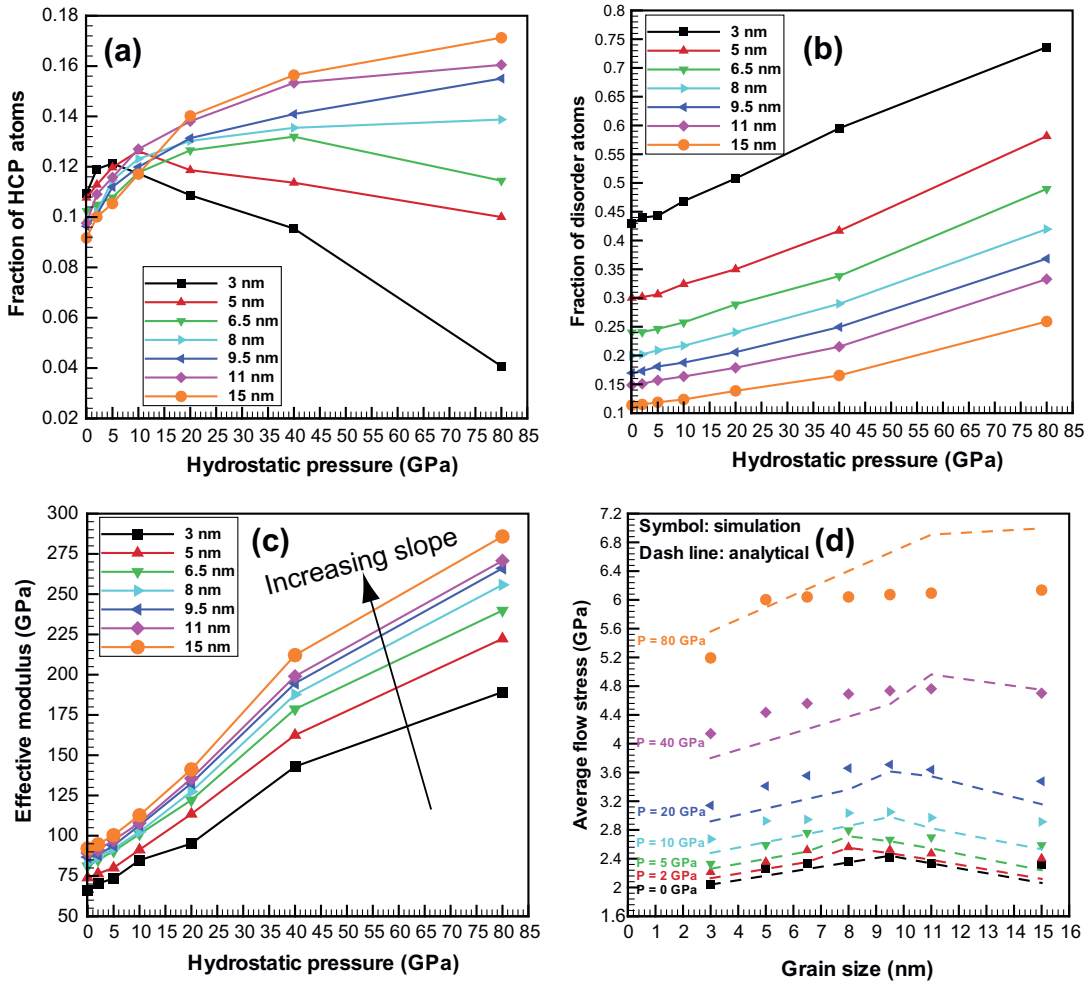

Fig. 5. (a) Fractions of HCP atoms at a strain of 10% as a function of hydrostatic pressure for various grain sizes; (b) fractions of disorder atoms at a strain of 10% as a function of hydrostatic pressure for various grain sizes; (c) effective modulus as a function of hydrostatic pressure for various grain sizes; and (d) comparison of simulation and analytical results for the average flow stress.

increasing hydrostatic pressure, which is consistent with the results shown in Fig. 4(a).

In order to understand the trend observed in Fig. 4(b), the hydrostatic pressure effects on the dislocation activity, GB accommodation plasticity and effective modulus are shown in Fig. 5(a)–(c). Fig. 5(a) shows fractions of HCP atoms at a strain of 10% as a function of hydrostatic pressure for various grain sizes, in which fractions of HCP atoms are generally indictors of

partial dislocation activities. Fig. 5(b) shows fractions of disorder atoms at a strain of 10% as a function of hydrostatic pressure for various grain sizes, in which fractions of disorder atoms are generally indictors of GB accommodation such as GB diffusion and GB thickening. For all grain sizes, the disorder atoms for GB increase monotonically and similarly with increasing hydrostatic pressure. Fig. 5(c) shows effective modulus as a function of hydrostatic pressure for various grain sizes. Below the critical hydrostatic pressure, the dislocation behaviors increase with increasing hydrostatic pressure for all grain sizes and the dependency of effective modulus as a function of hydrostatic pressure is almost the same for all grain sizes, which should give rise to the position shifting of maximum strength towards lower grain sizes as suggested in the previous research [23]. However, above the critical hydrostatic pressure, the dislocation behaviors start to decrease with increasing hydrostatic pressure for small grain sizes, and continue to increase with increasing hydrostatic pressure for large grain sizes. The slopes of effective modulus as a function of hydrostatic pressure slightly increase with increasing grain size above the critical hydrostatic pressure. These two observations should turn around the position shifting direction of the maximum strength from towards lower grain sizes to towards larger grain sizes above the critical hydrostatic pressure as suggested in the previous paragraph, as observed in Fig. 4(b). In the present study, the flow stress based on the analytical model for the grain size with the maximum strength under various pressures will be taken as: $\sigma_{flow} = 0.5\sigma_{Disl} + 0.5\sigma_{GB}$, and the flow stress for other grain sizes under various pressures will be taken as: $\sigma_{flow} = \min(\sigma_{Disl}, \sigma_{GB})$. The model parameters α, d_0, d_1 will be taken as 0.04, 30 nm, 30 nm, respectively, based on previous research [23]. Then σ_0 can be estimated to be 1.8545 GPa when considering the simulated flow stress under 0 GPa for 3 nm grain size. Since the maximum strength happens at 9.5 nm grain size under 0 GPa, C can be determined by setting $\sigma_{Disl} = \sigma_{GB}$ under 0 GPa for 9.5 nm grain size. C is estimated to be 0.01584. The effective modulus $\overline{G}(d, P)$ will be fitted from Fig. 5(c). Then the analytical data for the average flow stress can be calculated and the results are shown in Fig. 5(d) and compared with simulation results. A good agreement can be found between the predictions of the analytical model and our simulation data.

Fig. 6(a) and (b) shows the simulated deformation patterns at a strain of 10% under various hydrostatic pressures in the NC Cu with grain sizes of 3 nm and 9.5 nm, respectively. Fig. 7 shows the simulated deformation patterns at a strain of 10% under various hydrostatic pressures in the NC Cu with grain sizes of 15 nm, only a thin slab along the x direction is shown for clarity. When the grain size is small (3 nm), the dislocation behaviors increase first with increasing hydrostatic pressure, and then become less dominated when the hydrostatic pressure increases further. However, the dislocation behaviors are observed to increase monotonically with increasing hydrostatic pressure when the grain size is large (9.5 nm and above). Even at the largest grain size investigated in the present study (15 nm), it is clearly observed that the plastic deformation behaviors are accommodated by partial dislocation behaviors and formation of intrinsic and extrinsic stacking faults (ISFs and ESFs), with a few of deformation twins (DT) inside the grains. In contrast to coarse-grained metals, in which plastic behaviors are accommodated by full dislocations nucleated from Frank–Read sources, partial dislocations nucleated from GBs of nanocrystalline metals travel across the grains on one of the available {1 1 1} slip planes, until annihilated at another GB and leaving SFs behind. Due to the interactions between partial dislocation and SFs, some dislocation networks are also formed inside the nanocrystal grain to accommodate plastic deformation. As indicated in Fig. 7, partial dislocation behaviors, formation of SFs and formation of dislocation networks are all enhanced with increasing hydrostatic pressure when the grain size is large (15 nm), which is consistent with results shown in Fig. 5.

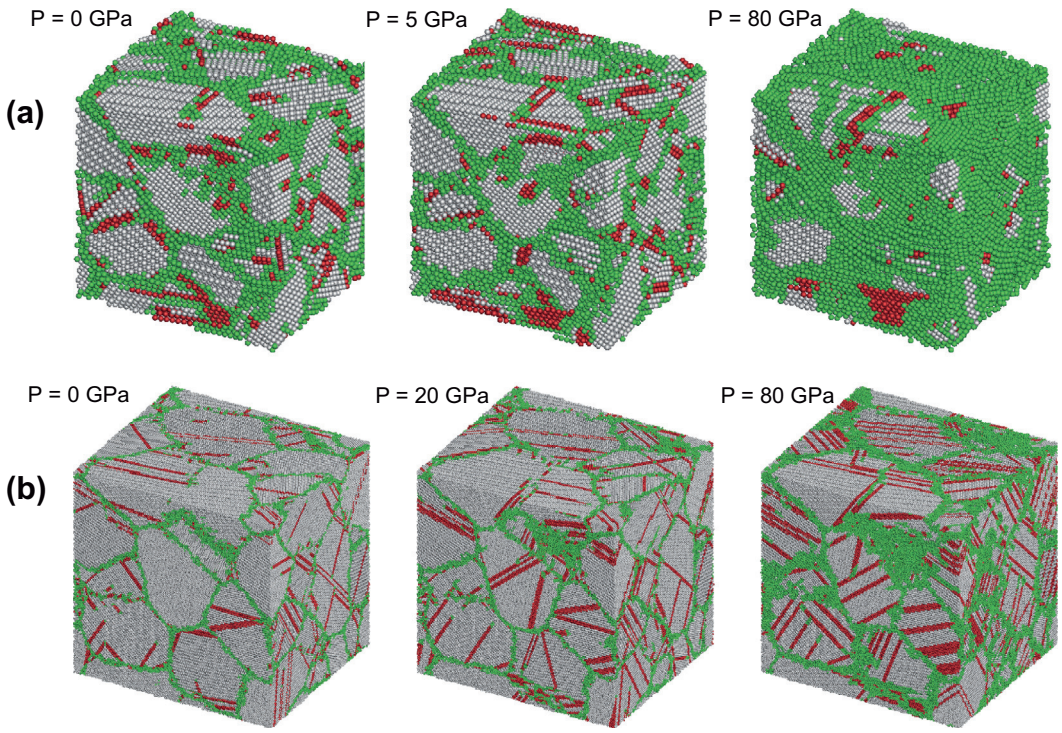

Fig. 6. The simulated deformation patterns at a strain of 10% in the NC Cu (a) with grain size of 3 nm under various hydrostatic pressures (P = 0, 5, 80 GPa); and (b) with grain size of 9.5 nm under various hydrostatic pressures (P = 0, 20, 80 GPa).

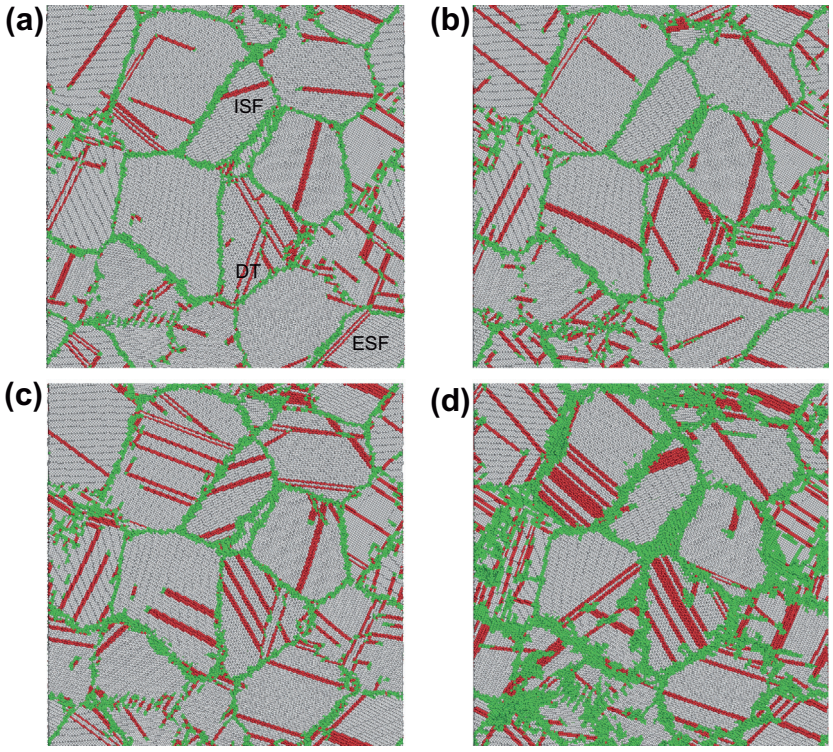

Fig. 7. The simulated deformation patterns at a strain of 10% in the NC Cu with grain sizes of 15 nm: (a) under hydrostatic pressure of 0 GPa; (b) under hydrostatic pressure of 2 GPa; (c) under hydrostatic pressure of 20 GPa; and (d) under hydrostatic pressure of 80 GPa. Only a thin slab along the *x* direction is shown for clarity. One typical intrinsic stacking fault (ISF), one typical extrinsic stacking fault (ESF) and one typical deformation twins (DT) are marked in Fig. 7(a).

GB thickening is observed to increase monotonically with increasing hydrostatic pressure for both grain sizes, and the NC Cu with grain size of 3 nm has the trend to become amorphous state after 10% strain compression when the hydrostatic pressure is as high as 80 GPa. The crystalline-to-amorphous transition has generally been observed during the high-strain-rate deformation processes [36–38]. Meyers et al. [36] reported the first observation on crystalline-to-amorphous transition in stainless steel inside a shear band formed under dynamics loading, which was attributed to a non-equilibrium solid-state amorphization process rather than melting. Amorphous structures were also observed by Zhang and Shim [37] in polycrystalline oxygen-free high conductivity copper severely deformed at high strain rate and liquid nitrogen temperature, in which they proposed that the amorphized regions were associated with the relative displacement between adjacent grains at their boundaries and the rotation of individual grains. More recently, a large region of amorphous phase was also identified in TWIP steel inside the shear band formed under high-strain-rate ballistic impact [38], and was attributed to melting inside the shear band. Although different mechanisms proposed [36–38], the high temperature rise due to adiabatic heating and extremely rapid cooling by heat dissipation should play an important role in the formation of amorphous region during the high-strain-rate deformation. However, the deformation temperature in the present simulations was controlled at 1 K, the small grain size and the ultra-high hydrostatic pressure should be the main factors for forming the amorphous state, which gives a new way to produce crystalline-to-amorphous transition.

4. Concluding remarks

MD simulations have been carried out to understand the interplay between hydrostatic pressure and grain size on the strength and the corresponding atomic-level deformation mechanisms in NC Cu. The flow stress of NC Cu was found to increase with increasing hydrostatic pressures for all grain sizes (3–15 nm). The position for maximum strength first shifts towards lower grain sizes with increasing hydrostatic pressure (0–5 GPa), and then shifts towards larger grain sizes as the hydrostatic pressure becomes even higher (5–80 GPa). Below the critical hydrostatic pressure, the dislocation behaviors increase with increasing hydrostatic pressure and the influence of hydrostatic pressure on effective modulus is almost the same for all grain sizes, which should give rise to the position shifting of maximum strength towards lower grain sizes. Above the critical hydrostatic pressure, the dislocation behaviors change to decrease with increasing hydrostatic pressure for small grain sizes, and continue to increase with increasing hydrostatic pressure for large grain sizes. Moreover, the hydrostatic pressure has slightly higher influence on the slopes of effective modulus for larger grain size above the critical hydrostatic pressure. These two observations should turn around the shifting direction of the maximum strength from towards lower grain sizes to towards larger grain sizes above the critical hydrostatic pressure. GB thickening is observed to increase monotonically with increasing pressure for all grain sizes, and the NC Cu with 3 nm grain size has the trend to become amorphous state under hydrostatic pressure of 80 GPa. The findings should provide insights for understanding the deformation physics of NC fcc metals under high hydrostatic pressures.

Acknowledgments

The authors would like to acknowledge the financial support of the National Key Basic Research Program of China (Grants Nos. 2012CB932203 and 2012CB937500) and NSFC (Grants Nos. 11002151, 11222224, 11072243 and 11021262). The simulations reported were performed at Supercomputing Center of Chinese Academy of Sciences.

Appendix A. Supplementary material

Supplementary data associated with this article can be found, in the online version, at http://dx.doi.org/10.1016/j.commatsci.2013.12.047.

References

[1] M.A. Meyers, A. Mishra, D.J. Benson, Prog. Mater Sci. 51 (2006) 427–556.
[2] M. Dao, L. Lu, R. Asaro, J.T.M. De Hosson, E. Ma, Acta Mater. 55 (2007) 4041–4065.
[3] H. Conrad, Metall. Mater. Trans. A 35 (2004) 2681–2695.
[4] C. Schuh, T. Nieh, T. Yamasaki, Scripta Mater. 46 (2002) 735–740.
[5] A. Giga, Y. Kimoto, Y. Takigawa, K. Higashi, Scripta Mater. 55 (2006) 143–146.
[6] J. SchiØtz, K.W. Jacobsen, Science 301 (2003) 1357–1359.
[7] D. Wolf, V. Yamakov, S. Phillpot, A. Mukherjee, H. Gleiter, Acta Mater. 53 (2005) 1–40.
[8] J. SchiØtz, F.D. Di Tolla, K.W. Jacobsen, Nature 391 (1998) 561–563.
[9] T.G. Nieh, J.G. Wang, Intermetallics 13 (2005) 377–385.
[10] Z. Qi, P. Sun, F. Zhu, Z. Wang, D. Peng, C. Wu, Surf. Coat. Technol. 205 (2011) 3692–3697.
[11] R. Masumura, P. Hazzledine, C. Pande, Acta Mater. 46 (1998) 4527–4534.
[12] Z. Cao, P. Li, H. Lu, Y. Huang, X. Meng, J. Phys. D-Appl. Phys. 42 (2009) 065405.
[13] Z.L. Pan, Y.L. Li, Q. Wei, Acta Mater. 56 (2008) 3470–3480.
[14] J.B. Jeon, B.J. Lee, Y.W. Chang, Scripta Mater. 64 (2011) 494–497.
[15] L. Lu, Y.F. Shen, X.H. Chen, L.H. Qian, K. Lu, Science 304 (2004) 422–426.
[16] L. Lu, X.H. Chen, X. Huang, K. Lu, Science 323 (2009) 607–610.
[17] A.J. Cao, Y.G. Wei, J. Appl. Phys. 102 (2007) 083511.
[18] X.Y. Li, Y.J. Wei, L. Lu, K. Lu, H.J. Gao, Nature 464 (2010) 877–880.
[19] Y.J. Wei, Phys. Rev. B 83 (2011) 132104.
[20] L.L. Zhu, H.H. Ruan, X.Y. Li, M. Dao, H.J. Gao, J. Lu, Acta Mater. 59 (2011) 5544–5557.
[21] F.P. Yuan, X.L. Wu, Phys. Rev. B 86 (2012) 134108.
[22] Y.T. Zhu, X.Z. Liao, X.L. Wu, Prog. Mater Sci. 57 (2012) 1–62.
[23] E.M. Bringa, A. Caro, Y.M. Wang, M. Victoria, J.M. McNaney, B.A. Remington, R.F. Smith, B.R. Torralva, H. Van Swygenhoven, Science 309 (2005) 1838–1841.
[24] B. Chen, K. Lutker, S.V. Raju, J. Yan, W. kanitpanyacharoen, J. Lei, S. Yang, H.-R. Wenk, H.-K. Mao, Q. Williams, Science 338 (2012) 1448–1451.
[25] L. Pizzagalli, J -L. Demenet, J. Rabier, Phys. Rev. B 79 (2009) 045203.
[26] S.N. Luo, T.C. Germann, T.G. Desai, D.L. Tonks, Q. An, J. Appl. Phys. 107 (2010) 123507.
[27] A.M. He, S.Q. Duan, J.L. Shao, P. Wang, S.N. Luo, J. Chem. Phys. 139 (2013) 074502.
[28] L. Miyagi, W. kanitpanyacharoen, P. Kaercher, K.K.M. Lee, H.-R. Wenk, Science 329 (2010) 1639–1641.
[29] D.-S. Xu, J.-P. Chang, J. Li, R. Yang, D. Li, S. Yip, Mater. Sci. Eng. A 387–389 (2004) 840–844.
[30] X. Dong, F. Liu, Y. Xie, W.Z. Shi, X. Ye, J.Z. Jiang, Comput. Mater. Sci. 65 (2012) 450–455.
[31] Y. Mishin, M.J. Mehl, D.A. Papaconstantopoulos, A.F. Voter, J.D. Kress, Phys. Rev. B 63 (2001) 224106.
[32] H. Tsuzuki, P.S. Branicio, J.P. Rino, Comput. Phys. Commun. 177 (2007) 518–523.
[33] F.P. Yuan, X.L. Wu, J. Appl. Phys. 113 (2013) 203516.
[34] B. Jiang, G.J. Weng, J. Mech. Phys. Solids 52 (2004) 1125–1149.
[35] A.C. Lund, C.A. Schuh, Acta Mater. 53 (2005) 3193–3205.
[36] M.A. Meyers, Y.B. Xu, Q. Xue, M.T. Pérez-Prado, T.R. McNelley, Acta Mater. 51 (2003) 1307–1325.
[37] B. Zhang, V.P.W. Shim, Acta Mater. 58 (2010) 6810–6827.
[38] N. Li, Y.D. Wang, R.L. Peng, X. Sun, P.K. Liaw, G.L. Wu, L. Wang, H.N. Cai, Acta Mater. 59 (2011) 6369–6377.